J Musculoskelet Neuronal Interact 2009; 9(4):215-224

Original Article

Hylonome

Devastation of bone tissue in the appendicular skeleton parallels the progression of neuromuscular disease

B.J. Lee[1], G.A. Cox[2], T.P. Maddatu[2], S. Judex[1], C.T. Rubin[1]

[1]Department of Biomedical Engineering, State University of New York, Stony Brook, New York 11794-2580, USA;
[2]The Jackson Laboratory, 600 Main Street, Bar Harbor, ME 04609, USA

Abstract

A mouse model of spinal muscular atrophy with respiratory distress (SMARD1) was used to study the consequences of neuromuscular degenerative disease on bone quantity and morphology. Histomorphometry and micro-computed tomography were used to assess the cortical and cancellous bone in the tibia, femur and humerus of adult neuromuscular degeneration (*nmd)* mice (up to 21w) and age-matched wild-type controls (WT). At 21w, the average lengths of the humerus, tibia and femur were 15%, 10%, and 10% shorter in the *nmd* mice, respectively. The midshaft of the humerus, tibia and femur of *nmd* mice had 41%, 47% and 34% less cortical bone than the WT. In the humeral, tibial, and femoral metaphyses of the *nmd* mice, there was 50%, 78%, and 85% less trabecular bone volume, and 58%, 92%, and 94% less trabecular connectivity than the WT. *NMD* cortical bone had less than half of the 42% active surface measured in the WT, yet the mineral apposition rate of those surfaces were similar between strains (*nmd*: 1.80μm·day^{-1}; WT: 2.05μm·day^{-1}). Osteoclast number and activity levels did not differ across strains. These data emphasize that neuromuscular degeneration as a result of immunoglobulin S-mu binding protein-2 (Ighmbp2) mutation will compromise several critical parameters of bone quantity and architecture, the most severe occurring in the trabecular compartment.

Keywords: Osteoporosis, Neuromuscular Disease, Bone, Spinal Muscular Atrophy (SMA), Spinal Muscular Atrophy with Respiratory Distress Type 1 (SMARD1)

Introduction

Osteoporosis can be a devastating secondary symptom of both acute and congenital neuropathic diseases[1]. For example, spinal muscular atrophy (SMA), a term that covers a host of genetic conditions with similar phenotypic alterations, is characterized by the progressive loss of alpha motor neurons in the spinal cord, followed by the atrophy of the skeletal muscles and subsequent osteopenia and elevated risk of fracture. The genetic mutation is most often in the survival motor neuron (*smn*) gene, but mutations in other genes can have the same pathophysiology[2].

A variant of SMA, spinal muscular atrophy with respiratory distress type 1 (SMARD1, also known as Distal spinal muscular atrophy type 1 (DSMA1)-Hum Mol Genet 2009 Apr 1; 18(7):1288-300. Epub 2009 Jan 20), is a congenital condition due to mutations in the ubiquitously expressed immunoglobulin S-mu binding protein-2 (*Ighmbp2*), causing the levels of functional protein to drop to 20-25% of the norm[3-18]. Referred in the literature under various names, such as cardiac transcription factor 1 and glial factor 1, *Ighmbp2* is a DNA helicase/ATPase protein which does not yet have a clearly defined function[17]. Phenotypically, SMARD1 is shown by a progressive paralysis and diaphragm paralysis due to the neuropathy, with secondary symptoms of fragility and deformities in the skeleton[4-6,8,10-16].

A spontaneous autosomal recessive mutation in the murine version of *Ighmbp2* was identified in C57BL/6J mice and helped to establish an animal model for SMARD1[17,18]. These neuromuscular degeneration mice (*nmd*) showed alpha motor neurons degeneration in the ventral horn of the spinal cord and consequent myopathy and atrophy of innervated skeletal muscle fibers[7,9]. In previous studies, neuronal degeneration of the motor neurons was visible via histology in the lumbar spinal cord and femoral quadriceps nerves as early as 10 days and 3 weeks, respectively[17]. Physical differences between the *nmd* and

Clinton T. Rubin is a founder of Marodyne Medical, LLC. No other authors have any potential or perceived conflicts of interest.

Corresponding author: Clinton T. Rubin, Ph.D., Department of Biomedical Engineering, State University of New York, Stony Brook, New York 11794-2580, USA
E-mail: Clinton.rubin@sunysb.edu

Accepted 15 September 2009

C57BL/6J mice were evident by the fourth week, with a distinct size difference between the *nmd* and B6 mice[7,17,18]. Between 4 to 7 weeks of age, significant differences in functional ability became evident between the *nmd* and their wild-type littermates, particularly in the rotarod and latency to fall tests, behavioral tests often used to quantify motor function in rodents.

Like the human condition, the muscle degeneration in the *nmd* mice begins in the hind limbs and progresses up the spinal column towards the forelimbs, with decreased levels of the functional protein in the central nervous system correlating to the onset of the disease phenotype. With this in mind, it is not clear if osteoporosis or bone loss is a primary consequence of the *nmd* mutation and therefore parallels the progression of neuromuscular degeneration or is a secondary outcome resulting from the reduced functional challenges to the musculoskeletal system.

Considering that the neuromuscular degeneration includes loss of motor function, it was proposed that a full characterization of the skeletal changes due to the *nmd* neuropathy would serve as a model of disuse in tandem with compromised skeletal maturation, and thus a means to study the extremes of reduced function on the growth of bone[19] and muscle[20]. It was hypothesized that the disuse state experienced by the *nmd* mice would lead to a significant reduction in all anabolic parameters involved in bone formation (e.g., reduced mineral apposition rate of osteoblasts), and a substantial increase in catabolic activity (e.g., resorption due to elevated osteoclast activity). Further, it was hypothesized that skeletal wasting would reflect a caudal to cranial progression of the neuropathy, with the humerus showing less disruption of bone mass and morphology than the tibia and femur, and thus indicate that the bone loss was secondary to the neuromuscular degeneration itself. Perhaps a detailed evaluation of the skeletal changes for this specific neurological dysfunction may ultimately provide insight in to the means by which these changes occur, and help identify targets for treatment of the condition.

Materials and methods

Animal Care: All procedures were reviewed and approved by the University's Animal Care and Use Committee. All C57BL/6J-*nmd* mice carried an immunoglobulin mu binding protein-2 (*Ighmbp2*) transgene expressed in cardiac myocytes to prevent death due to cardiac myopathy[21]. Due to the severe nature of the neurogenic atrophy and paralysis, rearing these animals to young adulthood proved very difficult, requiring that the experiment be run in two groups, represented by a total of ten *nmd* mice (8f, 2m). The age of the animals, following a 3w period of observation, ranged from 15-21w. To help maintain body heat, each *nmd* mouse was paired and housed with a non-*nmd* littermate of the same age and gender, with two exceptions. One male *nmd* mouse was housed with two male WT littermates and two female *nmd* littermates were housed with one WT littermate. Mice were weighed each day, 5 days a week. Qualitative behavioral observations of the *nmd* group, as compared to the WT were performed for $30 min \cdot d^{-1}$. All animals had unlimited access to rodent chow (22% protein & 5% fat content; RMH 3000, PMI Feeds, Inc, St. Louis, MO) and water. Water was available through an inverted water bottle with a drinking tube long enough for the *nmd* mice. Dry food from overhead bins and wet food in a plastic dish on the cage floor were checked daily to ensure unlimited access to food.

Measurements of dynamic parameters of bone remodeling were enabled through two IP injections of calcein (15 mg/kg, Sigma cat # C0875), performed at either days 6 & 16, or 10 & 19 of the protocol. All mice were euthanized on the 22nd day of observation. From the right limbs of all animals, the humerus, femur and tibia were dissected free and stored in 70% ethyl alcohol at -20°C. From the first set of animals, the soleus and tibialis anterior muscles, as well as the femur, tibia and humerus, were removed from the left limbs and stored in -80°C, while tissues from the left limbs of the second animals were stored in 10% formalin.

Micro-computed Tomography (μCT): Post-sacrifice, for both *nmd* and WT mice, the metaphysis of the right distal femur, proximal tibia and proximal humerus were scanned using μCT at 6μm resolution (Scanco Medical AG, Basserdorf Switzerland). The length of the bone was measured using the μCT scout view. A 1.5 mm region of the distal femur 0.4 mm proximal to the growth plate, and 0.84 mm region of the proximal tibia and humerus 0.2 mm distal to the growth plate were evaluated in terms of cortical bone area (mm^2), trabecular bone volume (%), connectivity density ($1/mm^3$), trabecular number (1/mm), spacing (mm), and thickness (mm). In addition, three 120 μm regions of the diaphysis of the femur, tibia and humerus diaphysis, centered at 40% (proximal), 50% (central), and 60% (distal) of the length of the bone, were evaluated for differences in cortical bone area (mm^2).

For the cortical regions of the metaphysis and diaphysis, total bone area (mm^2) was analyzed. For the trabeculae, the morphological characteristics analyzed included bone volume (BV), bone volume fraction (BV/TV), connectivity density (Conn D.), trabecular number (Trab N.), trabecular thickness (Trab Th.), and trabecular separation (Trab Sp.)[22]. Second moment of inertia calculations were determined for the anterior-posterior (Imin) and medial-lateral (Imax) axes for the central diaphysis region for the cortical bone area of the humerus, tibia and femur.

Histomorphometry: Post scanning, the right femur, humerus, and tibia were bisected with a diamond wafer saw and embedded in methylmethacrylate[23]. Once cured, the embedded bone was trimmed and 6 μm sections made in the longitudinal plane. Each section was slide mounted with a hybridization slip overnight, and mounted permanently with Eukett mounting medium and a 22 mm x 30mm glass cover slip, and allowed to dry overnight. Dynamic histo-morphometry was performed on the distal femur of *nmd* and WT, as measured using the calcein labels on the first set of mice (Osteometrics; Decatur, GA). Mineralizing surface area (MS) in the total bone surface area and the mineral apposition rate (MAR) was also established.

After storing the humerus and tibia in 10% formalin solution for 24 hours, the bones were bisected with a diamond wafer saw, and decalcified for 4d in a 1:1 solution of 5%

	nmd				Wild Type			
	cage code	sex	age (wks)		cage code	sex	age (wks)	
			start	end			start	end
Group 1	**5875 *nmd***	M	12	15	**5875-C**	M	12	15
	5876 *nmd*	F	13	16	**5876-C**	F	13	16
	5877 *nmd*	F	16	19	**5877-C**	F	16	19
	5878 *nmd*	M	13	16	**5878-C1**	M	13	16
	A5 *nmd*	F	12	15	**5878-C2**	M	13	16
	A6 *nmd*	F	12	15	**A**	F	12	15
Group 2	**9 *nmd***	F	18	21	**9 WT**	F	18	21
	10 *nmd*	F	18	21	**10 WT**	F	18	21
	11 *nmd*	F	18	21	**11 WT**	F	18	21
	12 *nmd*	F	18	21	**12 WT**	F	18	21
Mice are separated in the experimental groups 1 and 2. The ages were provided by the breeding facility, Jackson Laboratories (Maine).								

Table 1. Gender, age, and ID codes for the *nmd* and wild-type control mice.

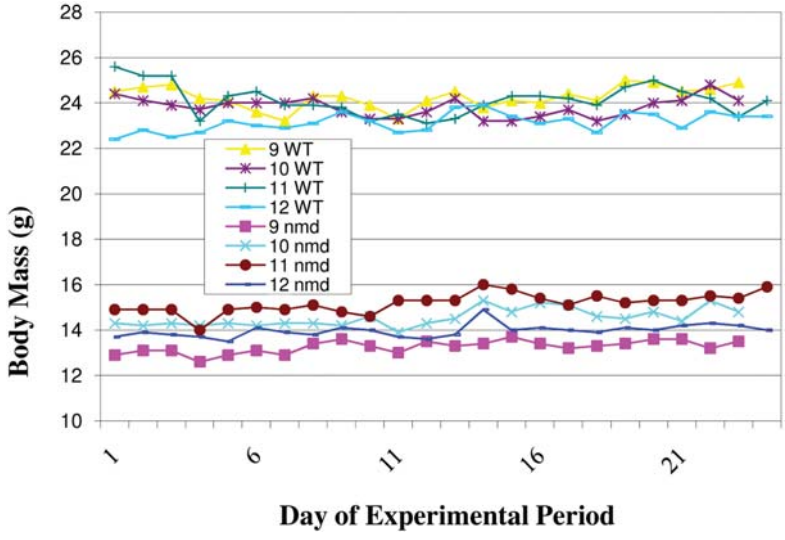

Graph 1. Body mass (g) of *nmd* and WT mice from the second group through the entire experimental period. The cluster of lines around 14g are the *nmd* mice and the cluster of lines around 24g are the WT mice. While a distinct gap persists between the two strains through the experimental period, this relationship does not change.

formic acid and 20% sodium citrate. Following decalcification, the distal and proximal portions of the humerus and tibia were embedded in glycol methacrylate (GMA) per the protocol of the JB-4 embedding kit (Polysciences, Inc. Cat # 00226) in the embedding molds (Polysciences, Inc.). Bones were sectioned at 6 μm on a Leica microtome (model # RM 2165), floated onto slides (Fisherbrand superfrost plus, cat # 12-550-15) and air dried. GMA sections were then stained for tartrate-resistant acid phosphatase (TRAP) activity using Liu's protocol[24], and counterstained with methyl green. Osteoclast activity of the cortical bone in the metaphyseal region of the left proximal humerus and tibia in *nmd* and WT mice was analyzed from the second set of animals. Three sections from each bone in each mouse were evaluated, and osteocyte density in the same region also being performed. Slides were blinded prior to analysis; three sections were analyzed per mouse.

Statistics: Mann-Whitney rank sum tests were used to compare the WT day 0 and 22 body mass, the day 22 body lengths, osteocyte cell counts per area, and the TRAP staining between groups. All other comparisons between groups, including be-

nmd				WT			
	Humerus	**Tibia**	**Femur**		**Humerus**	**Tibia**	**Femur**
5875	10.787	*	*	**5875 C**	12.250	17.688	16.262
A 6	9.818	*	14.350	**5876 C**	12.200	17.875	15.563
5876	10.562	15.439	13.850	**5877 C**	12.238	17.925	15.381
5877	10.488	16.800	14.300	**5878 C1**	12.377	17.950	15.394
5878	10.887	17.037	14.850	**5878 C2**	12.375	18.116	15.782
A 5	9.387	15.800	14.100	**A C**	12.425	18.147	15.844
9 *nmd*	10.438	15.987	13.705	**9 WT**	12.225	18.057	15.800
10 *nmd*	10.806	16.269	13.793	**10 WT**	12.294	18.194	15.769
11 *nmd*	10.212	16.263	14.475	**11 WT**	11.850	17.712	15.594
12 *nmd*	10.819	16.256	14.650	**12 WT**	11.939	17.863	15.262
Mean	10.420	16.231	14.230	**Mean**	12.217	17.953	15.665
SD	0.490	0.514	0.398	**SD**	0.187	0.175	0.291

** indicates a break at the growth plate. Measurements were taken post-mortem, using an electronic caliper to the thousandth decimal point. Average and standard deviations (SD) were of all available bones in both groups.*

Table 2. Absolute lengths (mm) of the humerus, tibia, and femur taken post-mortem.

	Proximal (40% of length)			**Central (50% of length)**			**Distal (60% of length)**		
	Humerus	**Tibia**	**Femur**	**Humerus**	**Tibia**	**Femur**	**Humerus**	**Tibia**	**Femur**
WT	0.66±0.11	0.68±0.03	0.89±0.05	0.53±0.02	0.56±0.03	0.77±0.05	0.50±0.05	0.65±0.08	0.74±0.05
nmd	0.35±0.05	0.34±0.04	0.55±0.06	0.31±0.06	0.30±0.03	0.51±0.05	0.33±0.01	0.34±0.04	0.51±0.05
% Diff.	47±19	51±7	38±9	44±7	47±8	34±8	34±10	48±13	32±10
p value	<0.001	<0.001	<0.001	<0.001	<0.001	<0.001	<0.001	<0.001	<0.001

Values are means ± SD, n=10 per group. Area was evaluated at three regions along the shaft, relative to 40, 50, and 60% of the total length of the bone. All data emphasize the severe differences between the areal properties of the WT (wild type) as compared to the nmd (neuromuscular degeneration) mice.

Table 3. Diaphyseal Bone Area (mm^2) for the humerus, tibia, and femur in WT and *nmd* mice.

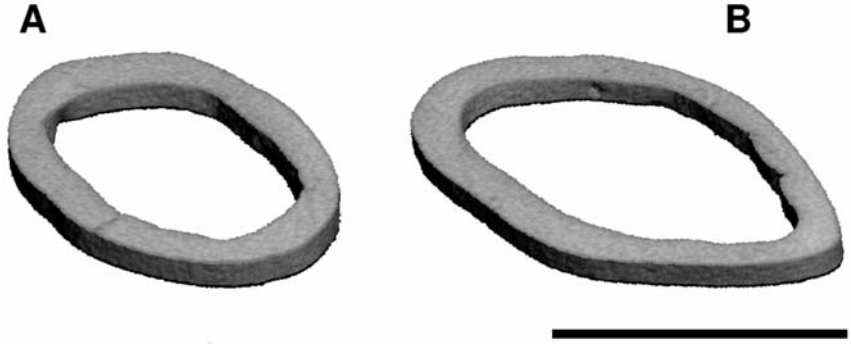

Figure 1. Representative image of microCT scans of the mid-diaphysis of the right femur of an *nmd* (A) and wild-type C57BL/6J mouse (B), each at 21 weeks of age. Areal properties indicate a 33±8% difference ($p<0.001$) in cross-sectional bone area between the *nmd* (A) wild-type C57BL/6J mice (B) at the midshaft. The second moments of area of the femoral midshaft, reflecting resistance to bending, was also 63±12% greater in the WT group ($p<0.001$). Scale bar is equal to 1.0 mm.

	Periosteal			Endosteal		
	Humerus	**Tibia**	**Femur**	**Humerus**	**Tibia**	**Femur**
WT	0.971±0.039	1.03±0.033	1.83±0.099	0.447±0.026	0.461±0.025	1.08±0.069
nmd	0.599±0.118	0.545±0.040	1.16±0.086	0.288±0.059	0.246±0.021	0.657±0.051
% Diff.	38±13%	47±5%	37±7%	36±14%	47±7%	39±8%
p value	<0.001	<0.001	<0.001	<0.001	<0.001	<0.001
Values are means ± SD, n=10 per group. Area was evaluated at the midpoint of the shaft, relative to 50% of the total length of the bone. All data emphasize the severe differences between the endocortical and periosteal areal properties of the WT (wild type) as compared to the nmd (neuromuscular degeneration) mice.						

Table 4. Central diaphysis periosteal and endocortical bone area (mm^2) of three long bones.

tween the two sets of *nmd* mice, were done using unpaired t-tests (two tailed) assuming unequal variances. Analysis of covariance (ANCOVA) could not be applied to adjust the p-values for the differences in body mass between control and *nmd* mice as prerequisites for the correlations between body mass and most skeletal variables were not met. Most bone variables violated the assumption of homogeneity of regression slopes or no correlation with body mass existed. Numerical data is presented as mean with standard deviation. A p-value <0.05 indicated a significant difference between the two strains of mice.

Results

Functional behavior: At day 21 of the study, representing an age range of 15-21w of all animals (Table 1), qualitative observations showed all *nmd* mice having functional use of their forelimbs, but near paralysis of the hind limbs, in stark comparison to their fully ambulatory WT littermates. The first set of *nmd* mice tended to stay in one location within their cages, and only occasionally pulled themselves to another location using their forelimbs. The second set was somewhat more active, and were observed grooming themselves, sitting on their haunches, feeding and drinking, and moving about their cage on a regular basis. However, behavioral variations in the genotype exist; and these functional disparities were neither unexpected nor could they be avoided.

Body Mass & Bone Length: At day 22, body mass of the first set of *nmd* mice was 14.5±0.99 g, 42% lower than the 25.0±2.3g measured in the WT (p<0.001 between *nmd* and WT). The second set of *nmd* mice and their WT counterparts were also weighed daily throughout the experimental period. While the two strains were completely independent from each other, their growth patterns were very similar (Graph 1). The length of the humerus, tibia, and femur (Table 2) from the *nmd* mice were 15%, 10% and 10% shorter than the WT (all p<0.001), respectively. There was no significant difference between the two sets of *nmd* mice in any of these parameters.

Micro-Computed Tomography: In the diaphyseal shaft, bone area measurements were taken at the locations where it was 40, 50 and 60% of the total length of the bone. As compared

	Bone Volume/Total Volume (%)		
	Humerus	**Tibia**	**Femur**
WT	7.3±1.0	7.8±1.1	5.6±1.3
nmd	3.6±1.7	1.7±0.6	0.8±0.6
% Difference	50±27	78±16	86±25
p-value	<0.0002	<0.0001	<0.0001
Values are means ± SD, n=10 per group. There is a far lesser volume of bone in the hindlimbs of the nmd strain versus the WT; an order of magnitude in the femur.			

Table 5. Bone volume fraction of the trabecular metaphysis of the distal femur, proximal tibia and proximal humerus.

to WT, the bone areas in the diaphyseal region of the *nmd* were smaller by at least 32% in all three bone and regions evaluated, as seen in Table 3 and Figure 1. P values were all less than 0.001 for the diaphyseal regions.

Areal measurements of the femur and tibia were compared to the humerus. The three diaphyseal regions were found to be significantly different between the humerus and the femur in both *nmd* and WT groups (Table 4). The 40, 50, and 60% regions of the WT humerus was 25±14%, 31±7%, and 33±9% lower in bone area relative to the femur (p<0.001 for all regions). In the *nmd*, the 40, 50, and 60% regions of humerus were 36±14%, 38±15%, and 35±11% lower, respectively, with respect to the femur (p<0.001 for all regions).

As compared to WT, trabecular volume fraction measurements in *nmd* were 50±27%, 78±16%, and 85±25% lower in the proximal humerus, proximal tibia, and distal femur (p<0.001 for all regions) as seen in Table 5. Connectivity parameters for the trabecular structure were evaluated in all three bones; however, more than half of the femora did not even have sufficient trabeculae to evaluate. All parameters were significantly lower in the *nmd* mice in comparison to the WT; the differences in the tibial and femoral connectivity density and trabecular number were far more severe than in the humerus (Tables 6, 7). Trabecular separation in the *nmd* mice were 52-

	Connectivity Density [1/mm³]			Trabecular Number [1/mm]		
	Humerus	**Tibia**	**Femur**	**Humerus**	**Tibia**	**Femur**
WT	93±40	84±24	114±50	3.7±0.49	3.8±0.65	3.6±0.79
nmd	39±27	6.8±6.1	8.2±10	2.7±0.67	2.2±0.24	1.9±0.38
% Diff.	58±52	92±30	93±45	29±22	41±18	47±24
p value	<0.004	<0.0001	<0.0001	<0.002	<0.0001	<0.0001
Values are means ± SD, n=10 per group. Connectivity density and trabecular number calculated via microCT of the trabecular metaphysis of the distal femur, proximal tibia and proximal humerus. The nmd strain has far less trabeculae than the WT as evidenced by the average number of connections between trabeculae per cubic millimeter and number of trabeculae per mm.						

Table 6. Connective density and trabecular number of the proximal humerus, tibia, and distal femur.

	Trabecular Separation [mm]			Trabecular Thickness [mm]		
	Humerus	**Tibia**	**Femur**	**Humerus**	**Tibia**	**Femur**
WT	0.27±0.04	0.27±0.05	0.29±0.06	0.039±0.004	0.044±0.003	0.037±0.005
nmd	0.40±0.11	0.46±0.050	0.54±0.10	0.034±0.005	0.042±0.006	0.027±0.004
% Diff.	65±28	58±16	52±22	13±16	4±16	27±17
p value	<0.01	<0.0001	<0.0001	<0.03	0.40	<0.0001
Values are means ± SD, n=10 per group. Trabecular separation and trabecular thickness calculated via microCT of the trabecular metaphysis of the distal femur, proximal tibia and proximal humerus. On average, the trabeculae are thinner and further apart in the nmd strain than the WT. The lesser BV/TV is explained by the increased distance between the sparse number of thinner trabeculae in the metaphysis of the nmd strain.						

Table 7. Trabecular separation and trabecular thickness of the metaphysis of the distal femur, proximal tibia and proximal humerus.

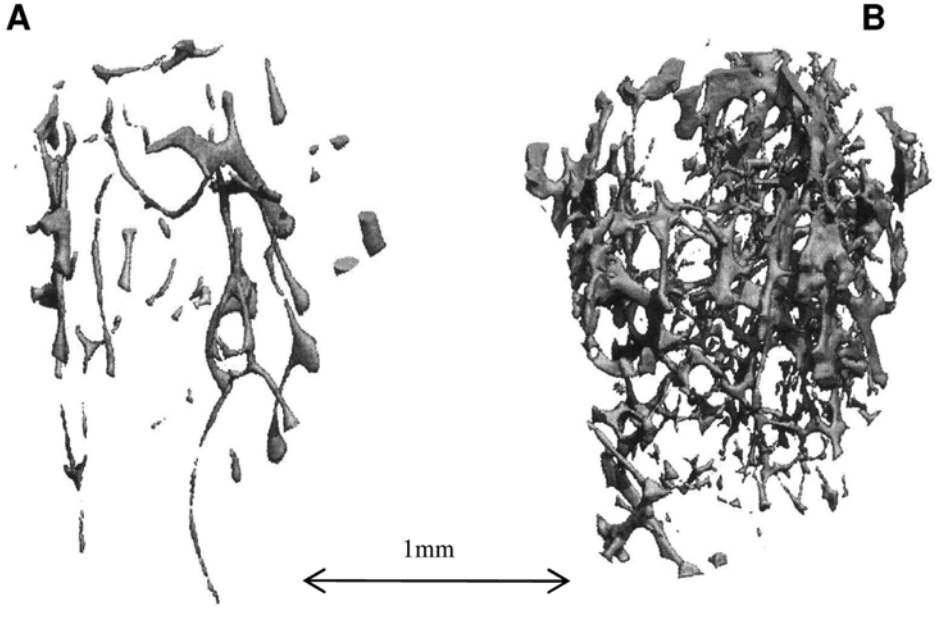

Figure 2. Representative images of microCT scans of the trabecular metaphysis from the right distal femur of the *nmd* mouse (A) and wild-type C57BL/6J mouse (B), each at 15 weeks of age. Compiled across groups, these images revealed an average of 95±35% ($p<0.001$) difference in the trabecular structure in both quality and quantity. Scale bar is equal to 1.0 mm.

	Imax - Moment of Inertia (mm^4)			Imin - Moment of Inertia (mm^4)		
	Humerus	**Tibia**	**Femur**	**Humerus**	**Tibia**	**Femur**
WT	0.089±0.010	0.077±0.008	0.231±0.026	0.038±0.003	0.058±0.004	0.122±0.014
nmd	0.037±0.036	0.020±0.004	0.085±0.014	0.016±0.005	0.017±0.003	0.058±0.009
% Diff.	58±43%	74±11%	63±12%	59±14%	71±8%	52±14%
p value	<0.002	<0.0001	<0.0001	<0.0001	<0.0001	<0.0001

Values are means ± SD, n=10 per group. Moments of inertia were calculated via microCT. The substantially lower maximum (Imax) and minimum (Imin) moments of inertias in the nmd strain in relation to the WT show that the long bones of the nmd are weaker than the WT, with a lower threshold for failure in bending.

Table 8. Maximum and minimum moments of inertia at the mid, or central diaphysis (50%) of the humerus, tibia, and femur.

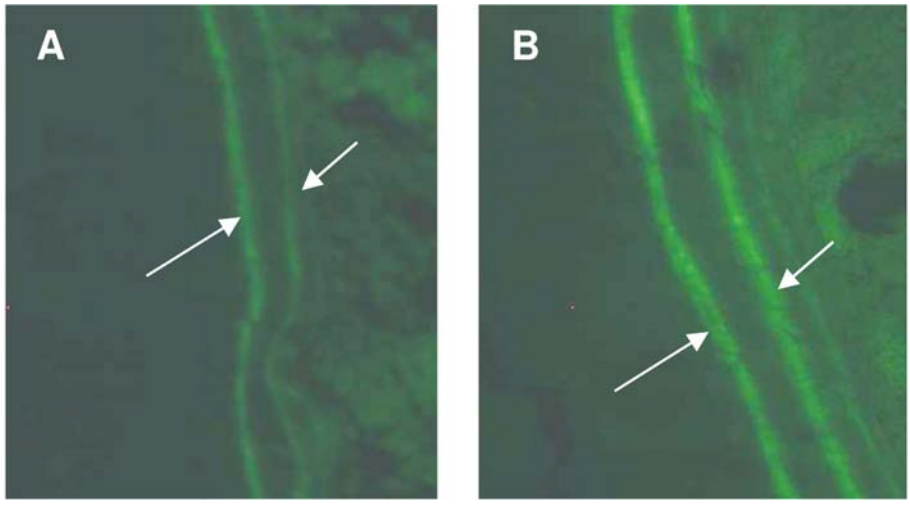

Figure 3. Representative images of double calcein labeling from the cortical shell of the metaphysis in the right distal femur of the *nmd* mouse (A) and wild-type C57BL/6J mouse (B), each at 15 weeks of age. Despite the large differences in bone quantity and quality between the two groups, the mineral apposition rate (i.e., distance between the labels) was not significantly different. Images taken at 20X.

65% greater than the WT strain (Table 7). The one exception to this was the trabecular number in the tibia (Table 6). The representative image shown in Figure 2 depicts the devastation of the trabecular bone in the metaphysis of the distal femur.

Differences in the cortical moments of inertia followed the caudal-cranial progression of the pathology, with the values for the WT always significantly greater than the *nmd* strain. The tibia showed the greatest variation between the two strains at 74±11% ($p<0.001$) about the medial-lateral axis (Imax), and 71±8% ($p<0.001$) difference about the anterior-posterior axis (Imin). Values for the femur and humerus also showed significantly large variation between the strains as seen in Table 8.

Histomorphometry: Only five of the ten *nmd* mice showed any evidence of double fluorescent label, and none had any evidence of fluorescent labels in the trabecular envelope. Therefore, all calcein labeling determination was performed in the metaphyseal region of the right distal femoral cortical shell. The percentage of single labeled surface area per bone surface area was 28±21% for the *nmd* group and 10±7 % for the WT ($p=0.03$). The *nmd* group had 21±22 % of the cortical bone surface showing a double label, essentially half of that measured in the cortical bone surface of the WT (42±8%; $p=0.02$). Photomicrographs showing double labeling in the WT and *nmd* mice are provided in Figure 3.

35±13 % of the cortical perimeter of *nmd* mice showed evidence of mineralized surface, 26% less cortical surface than the WT (47±7 %; $p=0.05$). However, in those regions that were undergoing bone formation, there were no significant differences measured between groups with the mineral apposition rate (MAR) or the bone formation rate per surface area (BFR/BS). The mineral apposition rate (MAR) for the *nmd* group was 1.8±1.2 $\mu m \cdot d^{-1}$, not significantly different from that measured in WT (2.1±0.1 $\mu m \cdot d^{-1}$; $p=0.52$). Bone formation rate per surface area (BFR/BS) was 308±237 $\mu m\ year^{-1}$ for the *nmd* was also similar to that measured in WT (352±70 $\mu m\ year^{-1}$; $p=0.9$).

Using TRAP activity staining to approximate osteoclast activity, the endosteal surface of the proximal humerus of the *nmd* showed 18±15% active surfaces, not significantly different from the 20±6% TRAP labeled surface measured in the WT. The proximal tibia showed a mean of 18±11 % and 12±5% labeled surface for the *nmd* and WT groups. No evidence of TRAP activity could be detected on the periosteal surface. In the cortical shell, there were 979±542 osteocytes/mm^2 for the *nmd* group, an osteocyte density that was not significantly different than the 811±140 osteocytes/mm^2 measured in the WT (p=0.5).

Discussion

As modeled by the *nmd* mouse, progressive neuropathy resulted in the significant devastation of both trabecular and cortical bone quantity and quality, and compromised several indices of skeletal growth. To a great degree, the comprised bone mass and morphology appeared to be a product of a significant reduction in the percent of bone surfaces active in bone formation. However, mineral apposition rate, where evident, appeared normal, indicating that the osteoblasts in the *nmd* mice were not dysfunctional; they just were not activated over any significant bone surface. Similarly, osteoclast activity and osteocyte density were similar between the *nmd* and WT mice, suggesting that the bone tissue itself was not in and of itself pathologic, and that instead, perhaps, the complications of *nmd* directly suppressed an existing signal to enable bone surfaces to activate. This perspective is supported by the contrast between static and dynamic histomorphometric patterns in bone tissue of *nmd* mice vs. normal mice subject only to disuse, where minimal mechanical loading in the latter results in the elevation of osteoclast activity and the suppression of mineral apposition rates[25,26]. These data suggest that reduced mechanical loading, in and of itself, is not responsible for the devastation of the skeleton in neuromuscular disease, and that these complications might best be approached by the introduction of anabolic therapies such as parathyroid hormone to help activate quiescent osteoblast surfaces[27].

Overall growth of *nmd* mice was also suppressed, as evidenced by reduced body mass, bone lengths and cross sectional areas as compared to the WT controls. The reduced weight reported here supports published data which show a body mass difference of nearly 50% between *nmd* and their WT littermates from 8 weeks of age and older[21], a potentially confounding variable that could not be eliminated by ANCOVA. In addition, the lengths of the long bones were markedly shorter in the *nmd* than the WT, which also undermines our hypothesized similarities to the skeletal complications of disuse, where longitudinal growth is not suppressed[28]. Extrapolating this to the human, clinical data on newborns with a range of neuropathic conditions do not show differences in length[1], but intrauterine growth retardation of SMARD1 patients has been reported in several case studies, again indicating distinct pathways of neuromuscular disease on the skeleton, and the distinction from disuse alone[8,13].

We had projected that the slowing of appositional growth of bone would correlate to regions with the greatest number of degenerate neurons, and thus differences in girth would be greatest in the bones of the hind limbs. In contrast to this hypothesis, no significant differences in areal properties were measured between fore and hind limbs, and certainly the differences relative to control in both the tibia and humerus were similar even though the "symptoms" of the neuropathy were more readily observable in the hindlimbs. That the forelimbs of the *nmd* mice were consistently used throughout the experimental protocol, as compared to the mobility of the hind limbs which markedly declined[9], provides further evidence that the devastation of the skeleton is not a 'simple' adaptation of bone tissue to reduced mechanical loading. That said, it is clear that the trabecular envelope in the tibia and femur was markedly more devastated than that measured in the humerus, suggesting distinct driving factors to define cortical versus cancellous morphology. Further supporting this, the *nmd* mice had substantially lower maximum and minimum moments of inertia versus the WT, indirectly indicating a lower threshold for bending failure in the mid-diaphysis of the long bones.

A number of limitations must be considered when extrapolating the results of these *nmd* mouse experiments to understanding the human condition. First and foremost, the *nmd* mouse is extremely fragile and proved extremely difficult to raise to this age, thus constraining the numbers of animals that could be evaluated. Further, a number of morphologic parameters in the *nmd* mouse, including body habitus, functional mobility and skeletal architecture, showed a wide range of measures within the pleomorphic limited number of animals examined, and emphasizes the spectrum of the disease. The two groups of *nmd* mice in this study had large differences in their functionality and behavior, but there were no significant differences between the two groups in the any of the bone parameters examined, which further supports a conclusion that the skeletal phenotype is a primary phenotype attributed to the genetic mutation, rather than a secondary response to widespread muscular dystrophy. And while the overall lifespan of the *nmd* mouse is somewhat limited, it is still longer than that studied here, and by simply reporting a single time point, it is important to stress that this study fails to address the temporal progression of the disease. This lack of a longitudinal study makes it impossible to rule out pathologies that may have occurred in the early stages of the *nmd* mice's lifespan, including high levels of osteoclast activity early in life. It must also be emphasized that the nutritional intake of the *nmd* and WT groups were not regulated, as it was essential to provide any and all food for the *nmd* mice, while at the same time it was not considered ethical to restrict food intake of the WT to approach pair feeding, creating the possibility of a nutritional deficiency or metabolic constraints as contributing factors[29]. And certainly only a select few skeletal locations and bone-tissue parameters were evaluated relative to the large numbers of factors that could have been effected by, or were effectors of, this disease. Again, the limited number of animals required that a limited number of key parameters be evaluated, leaving out assays such as transcriptional differences, cellular responses, or material and mechanical properties.

Originally, we had proposed the *nmd* mouse as a model of severe disuse, with the anticipation that the etiology of neuromuscular disease would result in a compromised skeleton through elevated osteoclast activity and a compromised formation rate in osteoblasts. Further, we anticipated that, because of the progression of the disease from caudal to cranial, the greatest complications would correlate to the hind limb, reflecting the regions with the greatest decline in function. While the bone mass and morphology were more severely compromised by neuromuscular degeneration than "simple" disuse, the data indicate that the majority of our hypotheses were incorrect: osteoclast activity in *nmd* mice remained similar to controls, mineral apposition rate – where evident – was normal, and the impact of the disease was similar in the diaphyseal shafts between the fore- and hind-limbs. At the same time, the trabecular response was perhaps less dramatic in the fore limbs, and provides some evidence for a sparing role of mechanical loading in slowing the tissue devastation. These data, while surprising, permit a conclusion that the skeletal complications of neuromuscular disease are systemic and direct, rather than a local and indirect response to reduced function. Regardless, the devastation of both bone mass and morphology certainly results in a greatly increased of risk of skeletal fracture, and clearly requires a targeted approach to build bone quality, perhaps through the restoration of active bone surfaces via the use of anabolic agents.

Acknowledgements

This work was supported by a grant from the National Institutes of Health (AR 49398) and AR049043 to GAC. We are grateful to the technical support in our animal facility for their enormous help wit the care and nurturing of these fragile mice.

References

1. Rodriguez JI, Palacios J, Garcia-Alix A, Pastor I and Paniagua R. Effects of immobilization on fetal bone development. A morphometric study in newborns with congenital neuromuscular diseases with intrauterine onset. Calcif Tissue Int 1988;43:335-9.
2. Crawford TO, Pardo CA. The neurobiology of childhood spinal muscular atrophy. Neurobiol Dis 1996;3:97-110.
3. Diers A, Kaczinski M, Grohmann K, Hubner C, Stoltenburg-Didinger G. The ultrastructure of peripheral nerve, motor end-plate and skeletal muscle in patients suffering from spinal muscular atrophy with respiratory distress type 1 (SMARD1). Acta Neuropathol (Berl) 2005; 110:289-97.
4. Viollet L, Zarhrate M, Maystadt I, Estournet-Mathiaut B, Barois A, Desguerre I, Mayer M, Chabrol B, LeHeup B, Cusin V, Billette De Villemeur T, Bonneau D, Saugier-Veber P, Touzery-De Villepin A, Delaubier A, Kaplan J, Jeanpierre M, Feingold J and Munnich A. Refined genetic mapping of autosomal recessive chronic distal spinal muscular atrophy to chromosome 11q13.3 and evidence of linkage disequilibrium in European families. Eur J Hum Genet 2004;12:483-8.
5. Rudnik-Schoneborn S, Stolz P, Varon R, Grohmann K, Schachtele M, Ketelsen UP, Stavrou D, Kurz H, Hubner C and Zerres K. Long-term observations of patients with infantile spinal muscular atrophy with respiratory distress type 1 (SMARD1). Neuropediatrics 2004;35:174-82.
6. Maystadt I, Zarhrate M, Landrieu P, Boespflug-Tanguy O, Sukno S, Collignon P, Melki J, Verellen-Dumoulin C, Munnich A and Viollet L. Allelic heterogeneity of SMARD1 at the IGHMBP2 locus. Hum Mutat 2004;23:525-6.
7. Maddatu TP, Garvey SM, Schroeder DG, Hampton TG and Cox GA. Transgenic rescue of neurogenic atrophy in the *nmd* mouse reveals a role for Ighmbp2 in dilated cardiomyopathy. Hum Mol Genet 2004;13:1105-15.
8. Guenther UP, Schuelke M, Bertini E, D'Amico A, Goemans N, Grohmann K, Hubner C and Varon R. Genomic rearrangements at the IGHMBP2 gene locus in two patients with SMARD1. Hum Genet 2004;115:319-26.
9. Grohmann K, Rossoll W, Kobsar I, Holtmann B, Jablonka S, Wessig C, Stoltenburg-Didinger G, Fischer U, Hubner C, Martini R and Sendtner M. Characterization of Ighmbp2 in motor neurons and implications for the pathomechanism in a mouse model of human spinal muscular atrophy with respiratory distress type 1 (SMARD1). Hum Mol Genet 2004;13:2031-42.
10. Garcia-Cabezas MA, Garcia-Alix A, Martin Y, Gutierrez M, Hernandez C, Rodriguez JI, Morales C. Neonatal spinal muscular atrophy with multiple contractures, bone fractures, respiratory insufficiency and 5q13 deletion. Acta Neuropathol (Berl) 2004;107:475-8.
11. Appleton RE, Hubner C, Grohmann K and Varon R. Congenital peripheral neuropathy presenting as apnoea and respiratory insufficiency: spinal muscular atrophy with respiratory distress type 1 (SMARD1). Dev Med Child Neurol 2004;46:576.
12. Pitt M, Houlden H, Jacobs J, Mok Q, Harding B, Reilly M and Surtees R. Severe infantile neuropathy with diaphragmatic weakness and its relationship to SMARD1. Brain 2003;126:2682-92.
13. Grohmann K, Varon R, Stolz P, Schuelke M, Janetzki C, Bertini E, Bushby K, Muntoni F, Ouvrier R, Van Maldergem L, Goemans NM, Lochmuller H, Eichholz S, Adams C, Bosch F, Grattan-Smith P, Navarro C, Neitzel H, Polster T, Topaloglu H, Steglich C, Guenther UP, Zerres K, Rudnik-Schoneborn S and Hubner C. Infantile spinal muscular atrophy with respiratory distress type 1 (SMARD1). Ann Neurol 2003;54:719-24.
14. Felderhoff-Mueser U, Grohmann K, Harder A, Stadelmann C, Zerres K, Buhrer C and Obladen M. Severe spinal muscular atrophy variant associated with congenital bone fractures. J Child Neurol 2002;17:718-21.
15. Grohmann K, Schuelke M, Diers A, Hoffmann K, Lucke B, Adams C, Bertini E, Leonhardt-Horti H, Muntoni F, Ouvrier R, Pfeufer A, Rossi R, Van Maldergem L, Wilmshurst JM, Wienker TF, Sendtner M, Rudnik-

Schoneborn S, Zerres K and Hubner C. Mutations in the gene encoding immunoglobulin mu-binding protein 2 cause spinal muscular atrophy with respiratory distress type 1. Nat Genet 2001;29:75-7.
16. Grohmann K, Wienker TF, Saar K, Rudnik-Schoneborn S, Stoltenburg-Didinger G, Rossi R, Novelli G, Nurnberg G, Pfeufer A, Wirth B, Reis A, Zerres K and Hubner C. Diaphragmatic spinal muscular atrophy with respiratory distress is heterogeneous, and one form Is linked to chromosome 11q13-q21. Am J Hum Genet 1999;65:1459-62.
17. Cox GA, Mahaffey CL and Frankel WN. Identification of the mouse neuromuscular degeneration gene and mapping of a second site suppressor allele. Neuron 1998; 21:1327-37.
18. Cook SA, Johnson KR, Bronson RT and Davisson MT. Neuromuscular degeneration (*nmd*): a mutation on mouse chromosome 19 that causes motor neuron degeneration. Mamm Genome 1995;6:187-91.
19. Judex S, Garman R, Squire M, Donahue LR, Rubin C. Genetically based influences on the site-specific regulation of trabecular and cortical bone morphology. J Bone Miner Res 2004;19:600-6.
20. Midura RJ, Dillman CJ and Grabiner MD. Low amplitude, high frequency strains imposed by electrically stimulated skeletal muscle retards the development of osteopenia in the tibiae of hindlimb suspended rats. Med Eng Phys 2005;27:285-93.
21. Maddatu TP, Garvey SM, Schroeder DG, Zhang W, Kim SY, Nicholson AI, Davis CJ and Cox GA. Dilated cardiomyopathy in the *nmd* mouse: transgenic rescue and QTLs that improve cardiac function and survival. Hum Mol Genet 2005;14:3179-89.
22. Odgaard A. Three-dimensional methods for quantification of cancellous bone architecture. Bone 1997;20:315-28.
23. Xie L, Jacobson JM, Choi ES, Busa B, Donahue LR, Miller LM, Rubin CT, Judex S. Low-level mechanical vibrations can influence bone resorption and bone formation in the growing skeleton. Bone 2006;39:1059-66.
24. Liu C, Sanghvi R, Burnell JM, Howard GA. Simultaneous demonstration of bone alkaline and acid phosphatase activities in plastic-embedded sections and differential inhibition of the activities. Histochemistry 1987;86:559-65.
25. Sakata T, Sakai A, Tsurukami H, Okimoto N, Okazaki Y, Ikeda S, Norimura T, Nakamura T. Trabecular bone turnover and bone marrow cell development in tail-suspended mice. J Bone Miner Res 1999;14:1596-604.
26. Rantakokko J, Uusitalo H, Jamsa T, Tuukkanen J, Aro HT and Vuorio E. Expression profiles of mRNAs for osteoblast and osteoclast proteins as indicators of bone loss in mouse immobilization osteopenia model. J Bone Miner Res 1999;14:1934-42.
27. Poole KE, Reeve J. Parathyroid hormone - a bone anabolic and catabolic agent. Curr Opin Pharmacol 2005;5:612-7.
28. Matsumoto T, Nakayama K, Kodama Y, Fuse H, Nakamura T and Fukumoto S. Effect of mechanical unloading and reloading on periosteal bone formation and gene expression in tail-suspended rapidly growing rats. Bone 1998;22:89S-93S.
29. Cooper C, Westlake S, Harvey N, Javaid K, Dennison E, Hanson M.Review: developmental origins of osteoporotic fracture. Osteoporos Int 2006;17:337-47.